Research Article

iMedPub Journals
www.imedpub.com

Nano Research & Applications
ISSN 2471-9838

2021
Vol.7 No.9:45

Analysis and Electrochemical Capacitance of Single Walled Carbon Nanotubes (10, 4) Synthesized Via Chemical Vapour Deposition Method

Danlami UZ*, Nuraddeen Muhammad Bui, Bala Hassan, Aliyu Sa'ad and Aliyu Jabbo Bunzah

Department of Chemistry, School of Sciences, Adamu Augie College of Education, Argungu, Kebbi State, Nigeria

***Corresponding author:**
Danlami Umar Zuru

Department of Chemistry, School of Sciences, Adamu Augie College of Education, Argungu, Kebbi State, Nigeria.

E-Mail: duzuru2013@gmail.com

Citation: Danlami UZ, Bui NM, Hassan B, Sa'ad A, Bunzah AJ (2021) Analysis and Electrochemical Capacitance of Single Walled Carbon Nanotubes (10, 4) Synthesized Via Chemical Vapour Deposition Method. Nano Res Appl Vol.7 No.9:45

Abstract

Single walled carbon nanotubes are receiving considerable attention in the nanotechnology industry, especially in electronics, as efficient energy storing materials. However, obtaining these materials of desired chirality via chemical vapour deposition method has posed a persistent challenge for over twenty years. In the current report, single walled nanotubes (10, 4) were successfully grown via pyrolysis of C_6H_{14}/N_2 feedstock on Fe_2O_3/Al_2O_3 catalyst. Field emission scanning electron microscopy and high resolution transmission electron microscopy images showed bundled network of single walled carbon nanotubes and resulting analysis of the Raman profile for the sample showed consistency with the results established via Extended Tight Binding model. This was a suggestion that if this method is fully optimized, it may help alleviate the stated global challenge. Specific capacitance (F/g) of 242, 174 and 50, was recorded for the sample in the neutral, acidic and alkaline electrolytes, respectively, also suggesting promising potentials as electrodes for Pseudocapacitor and electrochemical double layer capacitor.

Keywords: SWCNT (10, 4); Selective synthesis; Chemical vapour deposition; Pseudocapacitor; Electrochemical double layer capacitor

Received: August 29, 2021; **Accepted:** September 09, 2021; **Published:** September 16, 2021

Introduction

Carbon Nanotubes (CNTs) are receiving a considerable attention in the nanotechnology industry, for research and technological applications, since their discovery in 1991, by Lijima [1]. This is due to their unique thermal, optical, mechanical, electronic and magnetic properties. They are basically classified as either Single Walled Carbon Nanotubes (SWCNTs) or Multi Walled Carbon Nanotubes (MWCNTs), formed by either rolling one graphene sheet or more than two graphene sheets, respectively, into a seamless cylinder. In comparison, SWCNTs has greater electronic properties than MWCNTs but very expensive to produce for commercial application [2]. SWCNTs have a length of a few micrometers and a diameter around 1–3 nm while Multi-walled CNTs have a length around 10 µm and a diameter of 5–40 nm; and are mainly composed of sp^2-hybridized carbon atoms, bonded in an hexagonal matrix.

Generally, CNTs are used in the field of nano-agriculture to enhance fast germination and overall growth of crops, which is predicted to be a boon for biomass production; in pharmacy and medicine due to their high surface area that is capable of adsorbing or conjugating with a wide variety of therapeutic and diagnostic agents (drugs, genes, vaccines, antibodies, biosensors, etc.); in energy and microelectronics due to excellent electrical conductivity and accessible pore sizes suitable for energy storage; in transport for the fabrication of lightweight and strong vehicle or aircraft body, strong and interactive windscreens with de-icing properties; and in composite materials to enhance physical and chemical properties such as toughness, durability, conductivity and strength [3,4]. The CNTs market is estimated to grow from USD 4.55 billion in 2018 to USD 9.84 billion by 2023, at a CAGR of 16.7%; commercially produced SWCNTs are rated at USD 2800/g and MWCNTs are rated at 1800/g [5]. These materials are therefore predicted to have future economic, technological and social prospects; consequently, huge amount of money is invested in their production worldwide.

And although advances were made in the field of CNTs synthesis

via chemical vapour deposition (CVD) method, however, mass production of these materials, especially, SWCNTs, has remained a global challenge for over 20 years [6]. This has limited the availability of these products in the research and technological industries. We have recently reported the selective synthesis of SWCN (11, 8), based on our reported theoretical model [7], the principle of which was used to design the Fe_2O_3/Al_2O_3 catalyst for the selective synthesis of SWCNT (10, 4).

Materials and Methods

Catalyst preparation

Equation 1 was used to estimate the amounts of precursor salts [$Fe(NO_3)_3.9H_2O$ and $Al(NO_3)_3.9H_2O$ (98%; Fisher)] needed to prepare the corresponding Fe_2O_3/Al_2O_3 oxide catalyst, respectively.

$$M_s = \frac{W_s \times O_m}{w_o \times p_s} \quad (1)$$

where , , , and are the amounts of precursor salt, molecular weight of precursor salt, amount of metal or support oxide needed to obtain the desired SWCNT, molecular weight of metal or support oxide and percentage purity of precursor salt, respectively. To prepare Cat.(10, 4), about 26 g of $Fe(NO_3)_3.9H_2O$ was dissolved in 100 mL distilled water in a conical flask, mixed thoroughly via stirring for 30 minutes, 23 g of $Al(NO_3)_3.9H_2O$ was then added into the resulting solution and the mixture stirred and left for another 24 hours, in order to achieve homogeneity. The nitrate solution was then dried for 48 hours at an adjusted temperature of 90°C. Resulting solid was calcined in a Vulcan furnace at 450°C under air circulation for two hours, at a heating rate of 5°C/min. The final product was finally cooled, manually grounded, stored in sample bottles and labeled as Cat (10, 4).

SWCNT (10, 4) synthesis

Synthesis was carried out using a split type horizontal furnace (LT Furnace STF-30-1200 model). The working temperature and nitrogen gas flow rate were fixed at 1000°C and 100 mL/min., respectively. Catalyst loading was about 0.5 gram, and pyrolysis time of the C_6H_{14}/N_2 feedstock on Cats. (10, 4) was set for 30 min at 0.06 mL/min. Resulting products were then cooled, scraped into sample bottles and labeled as SWCNT (10, 4).

Functionalization of SWCNT (10, 4)

About 50 mg of Cat. (10, 4) was mixed with 40 mL of 4 M NaOH solution and stirred with a magnetic stirrer for two hours at 50°C. Precipitated aluminum complex was decanted and resulting residues batched washed with distilled water to neutral via centrifugation. The solid samples were then dried and dissolved in a mixture of concentrated H_2SO_4/HNO_3 solution (3:1) ratio, ultra-sonicated for one hour at 60°C and batch washed to obtain a neutral solution. Resulting solid was finally dried for four hours at 150°C and stored in sample bottles before analysis [8].

Analyses of Cat. (10, 4)

The X-ray diffraction patterns of the samples were obtained using an XRD-6000 powder diffract meter of CuK_α radiation (λ=0.15406 Å) operated at 40kV and 30 mA at 4°C min^{-1}. Profiles of data were analysed using an X'Pert High score PAN analytical software version 1.0d, via Shearer equation. Field-Emission-Scanning Electron Microscopy (FESEM) and High Resolution Transmission Electron Microscopy (HR-TEM) images of the samples were obtained using an FEI Nova Nanosem 230 and a Zeiss EM 902A, respectively. Raman analysis of as-grown SWCNT (10, 4) was obtained with a WITec Alpha 300R Raman spectrometer, using a laser excitation wavelength of 532 nm, corresponding to 2.3 eV metallic resonant [8]. The resulting Radial Breathing Modes (RBMs) from the profile were used to estimate the diameter (d_t) and the band gap (E_{11}), using equations (2) and (3), respectively, [9,10].

$$d_t = \frac{248}{\omega RBM} \quad (2)$$

$$E_{11} = \frac{6a_{cc}\gamma_\bullet}{d_t} \quad (3)$$

Where , , and are respectively, the radial breathing mode, C-C distance (0.1421nm), nearest neighbor hoping parameter (2.9eV) and diameter.

Specific capacitance of SWCNT (10, 4) was investigated using an Auto lab PGSTAT204/FRA32M module, consisting of three-electrode cell. A Glassy Carbon Electrode (GCE) coated with the dispersed sample served as the working electrodes and tested in 1 M neutral, alkaline and acidic aqueous electrolytes, using KCl, KOH and H_2SO_4, respectively. The counter and reference electrodes were respectively, Pt. wire and Ag/AgCl/saturated. About 10 mg of sample was dispersed in 10 mL of distilled water and sonicated for 15 min. The glassy carbon electrode was first polished using alumina slurry and the adhered Al_2O_3 particles removed by washing with distilled water. Resulting electrode was then sonicated in ethanol water (50:50, v/v) solution and rinsed with distilled water and dried at 40°C [11]. About 10 µL of the sample suspension was coated on the bare GCE using a micropipette and left to dry at room temperature.

Cyclic voltammetry tests were set at scan rates of 0.01Vs^{-1}, 0.02Vs^{-1}, 0.03Vs^{-1}, 0.05Vs^{-1}, 0.1Vs^{-1} and 0.2Vs^{-1}; working current potentials were varied from -1 V to 1V, in the neural environment; -0.2 V to 0.6 V in alkaline aqueous solution and 0.0 to 1.0 V in acidic medium. Charge-discharge tests were conducted at around 1.0E-5 V to -1.0E-5 V. Quantitative evaluation of the charge storage ability of the CNTs were determined by the SWCNT electrode mass (m), potential window (ΔE) and the voltammetry charges (Q), from which the specific capacitance (C) of the CNT electrodes were calculated using equation 4,

$$C = \frac{Q}{\Delta E \times m} \quad (4)$$

The voltammetry charge (Q) is estimated from the sum of the anodic and cathodic charges, by dividing the integral of the CV curve with the CV scan rate [12], using an OriginPro 9.0 64 Bit Software.

Results and Discussion

Analysis of Cat. (10, 4)

Figure 1a displays a plotted profile of diffraction patterns of Cat. (10, 4). Prominent diffraction peaks appeared at 2Θ=24.2•, 33.3•, 35.6•, 41.0•, 49.6•, 54.2•, 62.6• and 64.2•, which respectively, corresponds to (012), (104), (110), (113), (024), (116), (214) and (300) reflections of hematite iron oxide, α-Fe_2O_3, phases, (JCPD no. 03-0664) [13-15]. This was a suggestion that at 450°C, the metal/support interaction was greatly enhanced. The FESEM image of the Catalyst sample shown in **Figure 1b** reveals pellets of nano sized particles with few agglomerations, suggesting high crystalline purity [16].

Analyses of SWCNT (10, 4)

Figure 2 displays plots of XRD profiles of SWCNT (10, 4). Peaks of graphitized carbon appeared at 2Θ (degree) range 26.3 – 26.6, 54.4 and 59.5, predicting reflections of hexagonal C (002), C (004) and C (102), respectively, (JCPDS file no. 75 – 1621) [17]. Peaks in the range 31.1-32.0 were attributed to reflection of Al_4C_3 (201) (JCPDS file no. 6-696) [18]. Reflections of α-Fe_2O_3 (104), (113) and (011) appeared at 33.5, 42.9 and 43.1, respectively, (ICDD file no. 10 – 10425) [18], while 37.8, 44.7 and 70.9 were peaks of γ''-FeN (111), (021) and (013), respectively, (JCPDS file no. 34 – 1) [19]. Reflections at 39.9 and 49.2 was attributed to Fe_3C (221) and (220), respectively (JCPDS file no. 6 – 696; 34 – 1), and those occurring in the range 45.2-45.9.4 were those of α-Fe (110) and Fe_3C (220) overlap (JCPDS file no. 6 – 696; 34 – 1) [20]. Peaks in the range 66.3-66.9 were reflections of α-Al_2O_3 (440) (ICDD file no. 10 - 0425) [21]. Reflections of C (002), C (102) and C (004) was a suggestion that the samples contained pure graphitized carbon atoms arranged in a hexagonal matrix structure [20].

Appearances of Al_4C_3, Fe_3C and γ''-FeN moieties on the sample SWCNTs may suggest that growth occurred on surface of the reduced catalyst, and the decomposition of C_6H_{14}/N_2 feedstock on the Fe_2O_3/Al_2O_3 catalyst matrixes might have been responsible for the production of atomic C, N and H. Bonding of N and C atoms to Fe metal was observed to proceed via strong p-d covalent bonding, and the charge transfer from Fe to these atoms is responsible for the molecular stability of the composites [2]. Carbides and nitrides composites were also reported to show synergetic effect on the chemical stability and corrosion resistance of the samples, which

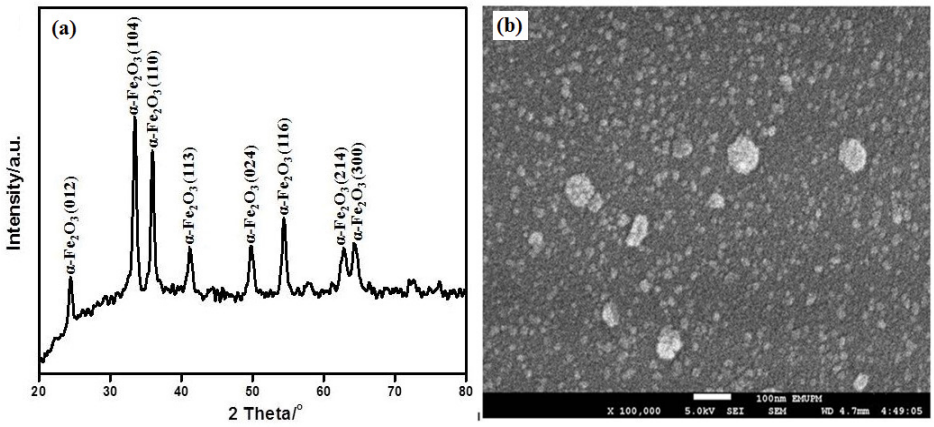

Figure 1 (a) XRD patterns of Cat. (10, 4) showing different phases of α-Fe_2O_3 and (b) FESEM images of Cat. (10, 4) revealing pellets of nano sized particles with few agglomerations suggesting high crystalline purity.

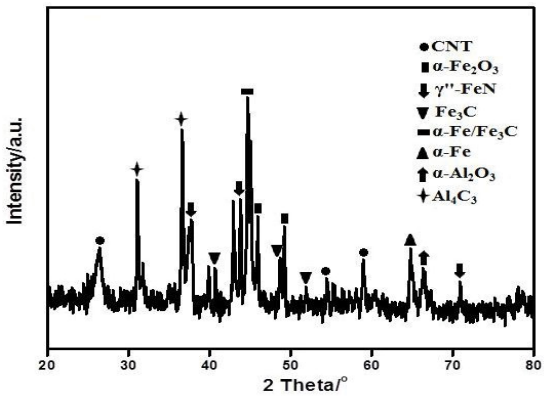

Figure 2 XRD profiles of SWCNT (10, 4) showing patterns of CNTs, metal carbides and nitrides.

results in better selectivity, catalytic capability and resistance to poisoning, as compare to their parents metal [22].

The FESEM and HR-TEM images of the SWCNT (10, 4) were displayed in **Figures 3a and 3b**, revealing dense forests of entangled tubes and rigid bundled array of SWCNTs, respectively. Complete dispersion of the sample SWCNT (10, 4) was not feasible, and may be attributed to the strong van der Waal's interaction (~ 500 eV) between the SWCNTs and π-π intertube stacking, which always resulted in the formation of large agglomerated bundles and ropes [23,24].

The plot of Raman profile of sample SWCNT (10, 4) obtained from Raman analysis is displayed in **Figure 4a**. The Radial Breathing Modes (RBMs) resonance (cm^{-1}) within the range 100-300, was a signature of single wall carbon nanotubes [9]. The D- and G- bands appeared at 1346cm^{-1} and 1578cm^{-1}, respectively, with an estimated ID/IG value of 0.5, indicating high levels of graphitization. The G'–band of the sample that appeared at 2691cm^{-1} and its strong intensity, signifies high level of purity and metallicity [9, 25]. The diameter and chiral angle of SWCNT (10, 4) estimated from the Raman RBMs are displayed in **Table 1**, in comparison with established ETB model results. Our model result showed acceptable deviations of 10%, from the RBMs and diameter of SWCNT (10, 4), respectively, reported by the ETB model [26]. The energy band gap of the sample was also observed to fall within the range metallic transitions (1.7-2.7 eV), which may suggest the metallicity of our sample SWCNTs [8].

The recorded deviations may be due to the inability of the ETB model to account for the curvature effects occurring in SWNTs with smaller diameter [27].

The FT-IR profile of the acid treated sample SWCNT (10, 4) is shown in **Figure 4b**. Peaks appearing in the range 1600 cm^{-1} – 1699 cm^{-1} correspond to stretching vibration from amide carbonyl functional group (-C=ONHR) [28], while peaks in the range 1408 cm^{-1} – 1412 cm^{-1} were due to stretching vibration of the amide group (N-H) [29]. Reflections from 1000 cm^{-1} to 1300 cm^{-1} and 3060 cm^{-1} - 3744 cm^{-1} were attributed to a bending vibration from -COOH moiety and O-H stretching vibration due to ambient atmospheric moisture or oxidation, respectively [30]. The –OH, -COOH and -C=ONHR functional groups were probably formed when the O and N atoms utilizes their electron pairs in the formation of delocalized π-bonds with the adjacent carbon atoms of the SWCNTs [20]. The 500 cm^{-1}-850 cm^{-1} peak range were attributed to α-Fe oxide phase while those around 390 - 450 cm^{-1} were designated to α-Al_2O_3 phase. Peaks in the range 500 cm^{-1}-850 cm^{-1} were attributed to α-Fe oxide phase while 390-450 cm^{-1} was designated to Al-C phase [31]. This outcome suggested successful functionalization of the sample SWCNT (10, 4), and was aimed at enhancing the wettability and therefore, the biocompatibility of the sample [32].

The estimated specific capacitance obtained for the sample SWCNT (10, 4) in the neutral, acidic and alkaline electrolytes at different scan rates are displayed in **Table 2.** From the table, our sample recorded highest specific capacitance (F/g) of 242, 174 and 50 in 1.0 M KCl, 1.0 M H_2SO_4 and 1.0 M KOH, respectively.

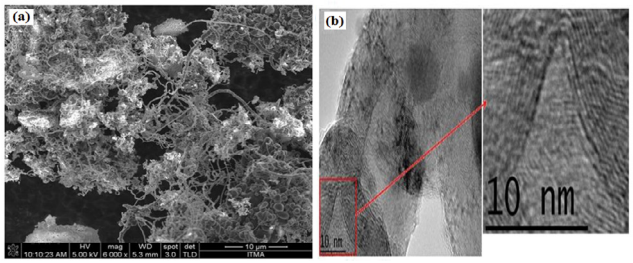

Figure 3 (a) FESEM image of SWCNT (10, 4) showing dense forest of entangled CNTs and (b) HR-TEM image of SWCNT (10, 4) showing rigid bundled array of aligned SWCNTs.

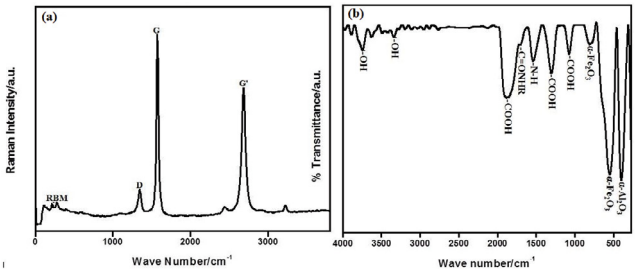

Figure 4 (a) Raman patterns showing RBMs of SWCNT (10, 4) and other important features and (b) FT-IR reflections of attached functional groups on matrix of SWCNTs (10, 4).

Table 1 Comparison between RBMs, diameter and E_{11} of SWCNTs (10, 4) with those established using ETB model.

Sample	Chiral Index (n, m)	ETB Equations			Modified Equations		
		RBM (cm-1)	Diameter (nm)	E11 (eV)	RBM (cm-1)	Diameter (nm)	E11 (eV)
SWCNT	(10, 4)	240	1.0	2.2	284	0.9	2.7

Table 2 Values of specific capacitance recorded of SWCNTs (10, 4) tested in 1.0 M KCl, 1.0 M H_2SO_4 and 1.0 M KOH electrolytes at different scan rates.

Scan Rate (V)	Specific Capacitance (F/g)		
	1.0 M HCl	1.0 M H_2SO_4	1.0 M KOH
	SWCNT (10, 4)	SWCNT (10, 4)	SWCNT (10, 4)
0.01	198	174	39
0.02	227	157	42
0.03	237	147	45
0.05	242	135	48
0.1	240	119	50
0.2	231	104	49

These results indicated that the electrochemical behavior of the sample was significantly enhanced by widening of the potential window of the electrolytes.

Figures 5a-5c are the plots of cyclic voltammograms of SWCNT (10, 4) tested in the neutral, acidic and alkaline electrolytes, respectively. Profiles of the sample in the neutral and acidic media showed enhanced current-potential responses with

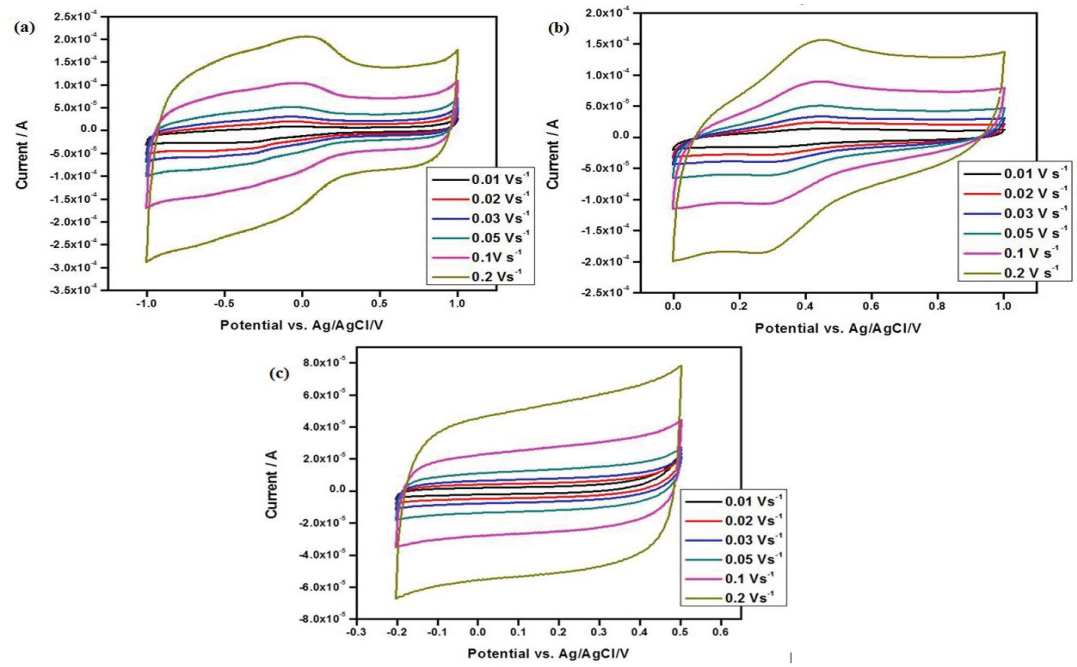

Figure 5 Plots cyclic voltammograms of SWCNT (10, 4) tested in (a) 1.0 M KCl, (b) 1.0 M H_2SO_4 and (c) 1.0 M KOH, showing enhanced current-potential response.

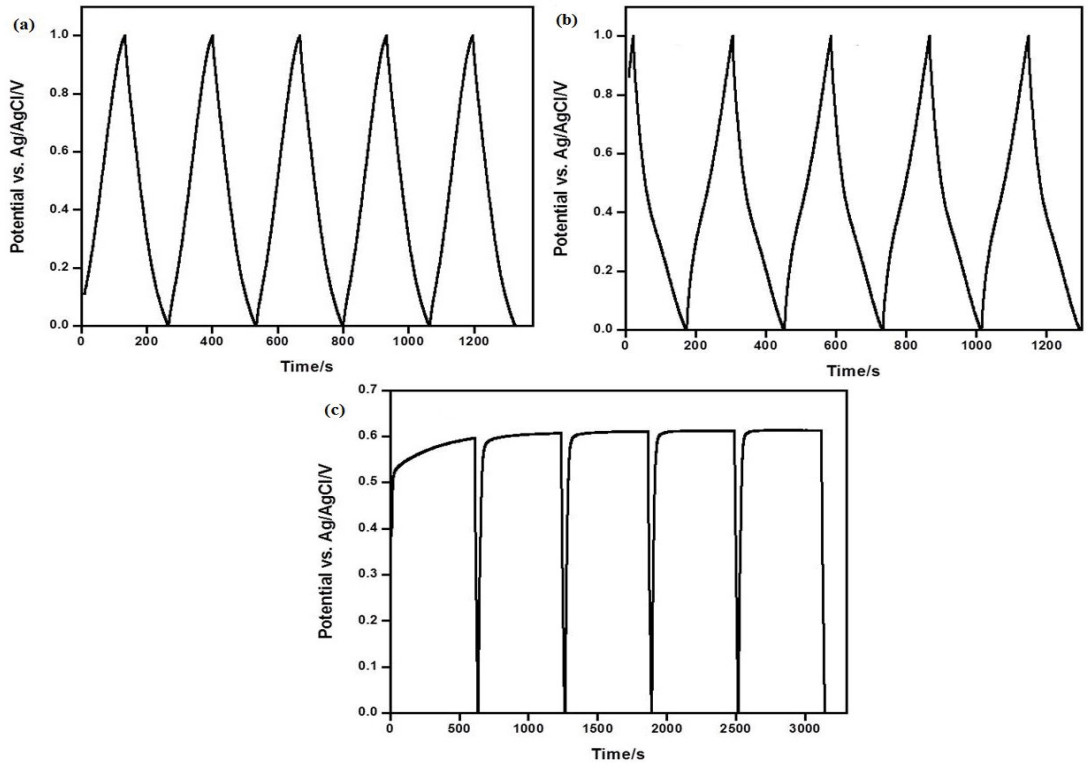

Figure 6 Plots of galvanostatic charge-discharge curves SWCNT (10, 4) tested in (a) 1.0 M KCl electrolyte, (b) 1.0 M H_2SO_4, showing straight triangular lines completed in 230 seconds and 180 seconds, respectively and (c) 1.0 M KOH indicated an average time-lag of 60 min before charging.

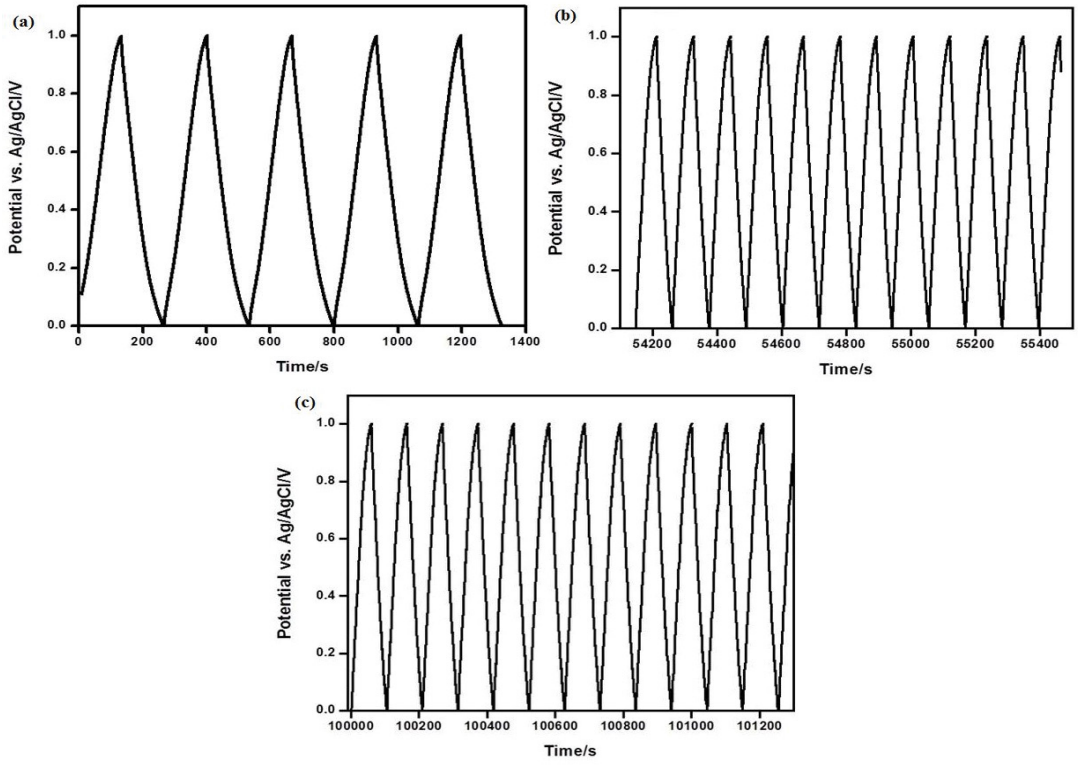

Figure 7 Plots of galvanostatic charge-discharge curves of SWCNT (10, 4) for 1000 cycle in 1.0 M KCl (a-c), revealing significant decrease in stability attributed to depletion of the electrode or attached functional groups.

pseudocapacitive behaviors, indicating high power and possible application for pseudocapacitor [33].

The essence of pseudocapacitance observed in both neutral and acidic media may be explained as follows: the strong electric field applied on the negatively charged cathode causes the bond lengths and bond angles of the attached functional groups to be in close contact with the H_3O^+ of the electrolytes, such that their electron clouds interact. This may facilitate the transfer of electrons from the functional groups to the O atom of the H_3O^+, converting it to a negatively charged center. In the alkaline medium, the samples also showed stable rectangular curves typical of an EDLC. The small size and large polarization intensity of K^+ (3.31 Å) hydrated ions might have facilitated the high charge density of the EDL. Large diffusion of the hydrated K^+ into the bulk solution of the EDL was probably enhanced by the attached functional groups which might have also inhibited their migration into the pores of the CNT.

These processes may account for the low capacitance, absence of redox peak in the CV and may also be responsible for the S-shaped CV in which the K^+ ions probably form the Inner Helmholtz Layer (IHP) with the electrode surface [34]. Resulting charge-discharge profiles of the electrodes in the neutral and acidic electrolytes revealed triangular straight lines and occurred in an average of 200 seconds, as shown in **Figures 6a and 6b,** respectively, suggesting possible application as pseudocapacitor electrode. In the alkaline medium, the resulting charge-discharge curves indicated an average time-lag of 60 min. before charging, as shown in **Figure 6c**, which suggests poor storage capability.

To estimate the long-term stability of the sample SWCNT (10, 4), 10 µL was investigated in 1.0 M KCl for 1000 cycles. Figure 7 were plots of the galvanostatic charge-discharge, in which an initial charge-discharge occurred in about 200 seconds in the first 100 cycles (**Figure 7a**) and decreased to about half the time in the first 500 and 1000 cycles, as shown in **Figures 7b and 7c**, respectively. It took a total of about 28 hours to complete the 1000 cycles.

Although a significant decrease was recorded, the sample electrode may be regarded as sustaining stable cycling process on the basis that it was a binder-free experiment.

Conclusion

Sample of SWCNT (10, 4) was synthesized based on our model principle and the physico-chemical properties of the sample shows acceptable conformity with established experimental results. The product has also demonstrated promising capability as pseudocapacitor electrode. It is hoped that an in-depth optimization of parameters involved in this method may serve to alleviate.

Acknowledgement

The funding by the Adamu Augie College of Education, Kebbi-State, Nigeria, is hereby acknowledged and appreciated; however, all ideas contained in this manuscript reflect the decision of the authors alone.

References

1 Lijima S (1991) Helical microtubules of graphitic carbon. Nature 354: 56-58.

2 Yap HY, Ramaker B, Sumant AV, Carpick RW (2006) Growth of mechanically fixed and isolated vertically aligned carbon nanotubes and nanofibers by DC plasma-enhanced hot filament chemical vapor deposition. Diam Relat Mater 15: 1622-1628.

3 Azam A, Fujiwara T, Shimoda T (2013) Significant capacitance performance of vertically aligned single-walled carbon nanotube super capacitor by varying potassium hydroxide concentration. Int J Electrochem Sci 8: 3902-3911.

4 Jiang D, Meng D, Wu J (2011) Density functional theory for differential capacitance of planar electric double layers in ionic liquids. Chem Phys Lett 504: 153-158.

5 Liu B, Wu F, Gui H, Zheng M, Zhou C, et al. (2017) Chirality-controlled synthesis and applications of single-wall carbon nanotubes. ACS Nano 11: 31-53.

6 Zuru DU, Zainal Z, Hussein MZ, Jaafar AM, Lim HN, et al. (2018) Theoretical and experimental models for the synthesis of single walled carbon nanotubes and their electrochemical properties. J ApplElectrochem.

7 Weng Z, Liu W, Yin LC, Fang R, Altman EI, et al. (2015) Metal/oxide interface nano-structures generated by surface segregation for electro catalysis. Nano Lett 15: 7704-7710.

8 Dresselhaus MS, Dresselhaus G, Saito R, Jorio A (2005) Raman spectroscopy of carbon nanotubes. Phys Rep 409: 47-99.

9 Pimenta MA, Marucci A, Empedocles JA, Bawendi MG, Hanlon EB, et al. (1998) Raman modes of metallic carbon nanotubes. Phys Rev B 58: 1-4.

10 Jain R and Sharma S (2011) Glassy carbon electrode modified with multi-walled carbon nanotubes sensors for the quantification of antihistamine drug Pheniramide in solubilized systems. Res J Chem Sci 1: 137-142.

11 Chen JH, Li WZ, Wang DZ, Yang SX, Wen JG, et al. (2002) Electrochemical characterization of carbon nanotubes as electrode in electrochemical double-layer capacitors. Carbon 40:1193-1197.

12 Liu P, He S, Wei H, Wang J, Sun C, et al. (2015) Characterization of α-Fe_2O_3/γ-Al_2O_3 catalysts for catalytic wet peroxide oxidation of m-cresol. Ind Eng Res 54: 130-136.

13 Gulshan F, Okada K (2013) Preparation of alumina-iron oxide compounds by co-precipitation method and its characterization. Am. J Mater Sci 1: 6-11.

14 Qin C, Lu X, Yin G, Jin Z, Tan Q, et al. (2011) Study of activated nitrogen-enriched carbon and nitrogen-enriched carbon/carbon aerogel composite as cathode materials for supercapacitors. Mater Chem Phys 126: 453-458.

15 Hermanek M, Zboril R, Medrik I, Pechousek J, Gregor C, et al. (2007) Catalytic efficiency of iron (III) oxides in decomposition of hydrogen peroxide: Competition between the surface area and crystallinity of nanoparticles. J Am Chem Soc 129: 10929-10936.

16 Kumar BV, Thomas R, Mathew A, Rao GM, Mangalaraj D, et al. (2014) Effect of catalyst concentration on the synthesis of MWCNT by single step pyrolysis. Adv Mater Lett 5: 543–548.

17 Yu WJ, Hou PX, Zheng LL, Li F, Liu C, et al. (2010) Preparation and electrochemical property of Fe_2O_3 nano particles filled carbon nanotubes. Chem. Commun 46: 8576-8578.

18 Dumee L, Sears K, Schutz J, Fim A, Duke M, et al. (2013) Influence of sonication temperature on the debundling kinetics of carbon nanotubes in propan-2-ol. Nanomaterials 3: 70–85.

19 Krisyuk V, Gleizes AN, Aloui L, Turgambaeva A, Sarapata B, et al. (2010) Chemical vapour decomposition of iron, iron carbides and iron nitride films from amidinate precursors. J Electrochem Soc 157: D454 – D461.

20 Arefin S (2013) Empirical equation based chirality (n, m) assignment of semiconducting single wall carbon nanotubes from resonant Raman scattering data. Nanomaterials 3:1-21.

21 Ham DJ, Lee JS (2009) Transition metal carbides and nitrides as electrodes materials for low temperature fuel cells. Carbon **7**:346.

22 Oki A, Adams L, Luo Z, Osayamon E, Biney P, et al. (2008) Functionalization of single-walled carbon nanotubes with N-[3-(trimethoxysilyl)Propyl]ethylenediamine and its Cobalt complex. J PhysChem Solids 69:1194-1198.

23 Britz DA and Khlobystov AN (2006) Non-covalent interactions of molecules with single walled carbon nanotubes. Chem Soc Rev 35:637-659.

24 Lehman JH, Terrones M, Mansfield E, Hurst KE, Meunier V, et al. (2011) Evaluating the characteristics of multiwall carbon nanotubes. Carbon 49: 2581-2602.

25 Nwoye CI and Ndlu S (2009) Model for predictive analysis of the concentration of phosphorus removed during leaching of iron oxide ore in sulphuric acid solution J. of Minerals and Materials Characterization and Eng 8: 261-269.

26 Somada H, Hirahara K, Akita S, Nakayama Y (2009) A molecular linear motor consisting of carbon nanotubes. Nano Lett 9: 62−65.

27 Tessonier JP, Su DS (2011) Recent Progress on growth mechanism of carbon nanotubes: A review. ChemSuschem 0000: 6-11

28 Heckert Jz, Uber IC, Whitaker CM (2007) Synthesis of amide functionalized carbon nanotubes. United States (U.S) Naval Academy (USNA)

29 Razali MH (2016) Physicochemical properties of Carbon Nanotubes (CNTs) synthesized at low temperature using simple hydrothermal method. Int J Appl Chem 12: 273-280.

30 Trivedi MK, Tallapagada RM, Branton A, Trivedi D, Nayak G, et al. (2015) Characterization of physical and structural properties of aluminum carbide powder: Impact of biofield treatment. J Aeronaut Aerospace Eng 4:1000-1042.

31 Hou P, Liu C, Cheng H (2008) Purification of carbon nanotubes. Carbon 46: 2003-2025.

32 Zhong C, Deng Y, Qiao J, Hu W, Zhang L, et al. (2015) A review of electrolyte materials and compositions for electrochemical supercapacitors. Chem Soc Rev 44: 7484-7920.

33 Tansel B, Sager J, Rector T, Garland J, Strayer RF, et al. (2006) Significance of hydrated radius and hydration shells on ionic permeability during nanofilteration in deep end and cross flow modes. Sep Purif Technol 51: 40-47.

34 Zhao Y, Hao M, Wang Y (2016) Effect of electrolyte concentration on the capacitive properties of NiO electrode for supercapacitors,Journal Solid State Electrochem. 20: 321- 329.